Gut Microbiota-Dependent Choline Metabolism Drives Mammary Gland Lipid Redistribution via Microbial Metabolites

Lily Liu[1, 2], Mengxue Hu[1], Min Yan[1], Songlin Liu[1], Weiqi Wang[1], Xu Luo[1]*, Qin Zhang[3]*, Jinhai Wang[2, 4]*

1. College of Biological and Food Engineering, Southwest Forestry University, Kunming 650224, China;
2. The Roslin Institute, University of Edinburgh, Edinburgh EH25 9RG, UK
3. College of Animal Science and Technology, Shandong Agricultural University, Tai'an 271018, China
4. College of Animal Science and Technology, Northwest A & F University, Yangling 712100, PR China

*Correspondence: jwang7@ed.ac.uk, qzhang@cau.edu.cn, luoxu@swfu.edu.cn

College of Animal Science and Technology, Northwest A & F University, Yangling 712100, PR China;

College of Animal Science and Technology, Shandong Agricultural University, Tai'an 271018, China; College of Biological and Food Engineering, Southwest Forestry University, Kunming 650224, China.

The Roslin Institute, University of Edinburgh, Edinburgh EH25 9RG, UK

Supplementary Figures

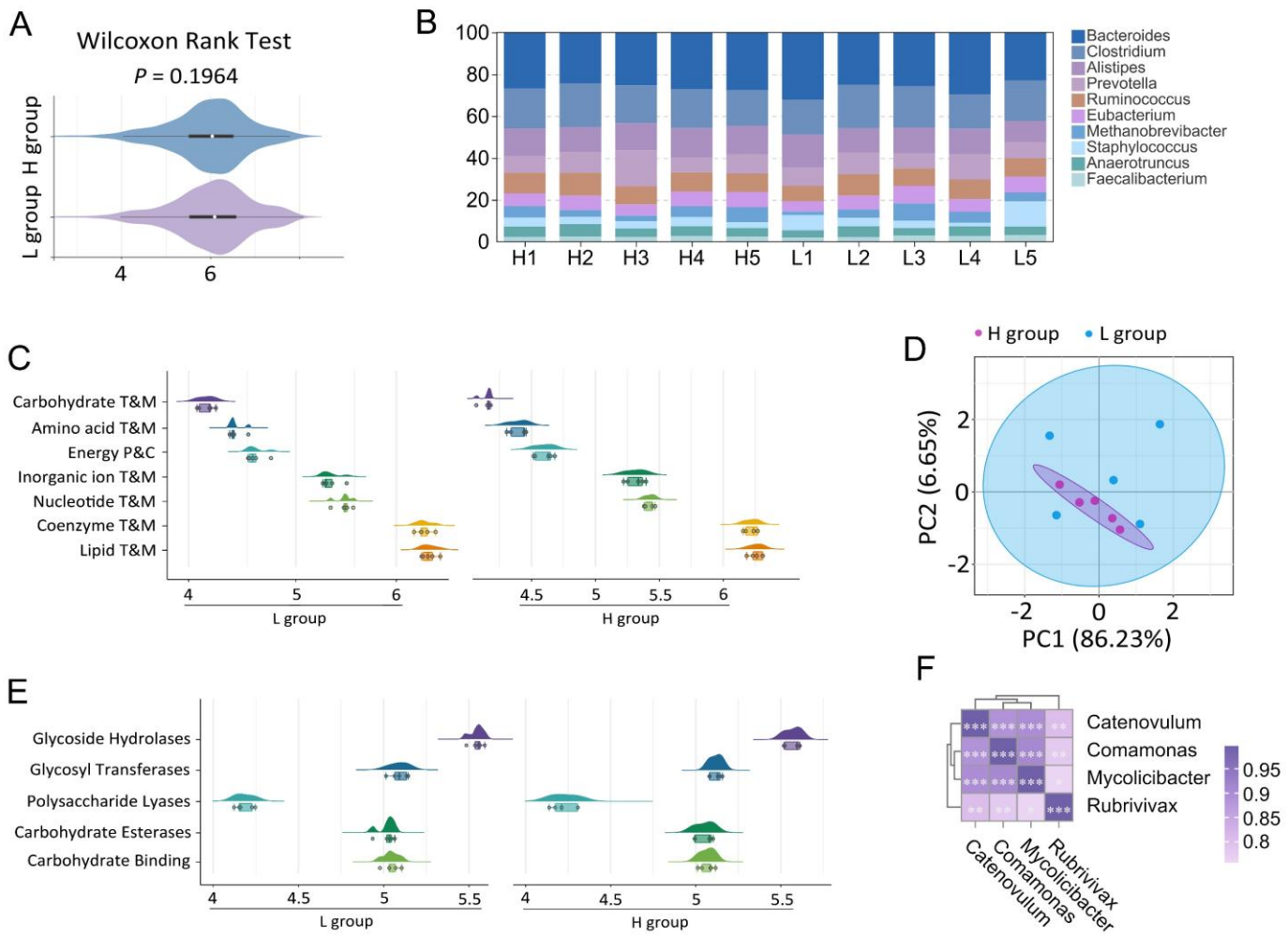

Figure S1. Functional and compositional differences in microbial communities between high (H) and low (L) milk fat percentage, related to Figure 1.

(A) Violin plot comparing overall microbial functional abundance between H and L groups (Wilcoxon rank test, $P = 0.1964$). **(B)** Stacked bar plots representing the relative abundance of gut microbial genera across individual samples from H (H1–H5) and L (L1–L5) groups. **(C)** Functional annotation of microbial communities showing group-specific differences in major metabolic pathways, including carbohydrate transport and metabolism (T&M), amino acid T&M, energy production and conversion (P&C). **(D)** Principal component analysis (PCA) based on functional profiles reveals clear separation between H and L groups along PC1 (86.23%). **(E)** Distribution of major CAZyme (carbohydrate-active enzyme) families, including glycoside hydrolases, glycosyl transferases, and polysaccharide lyases, between H and L groups. **(F)** Heatmap of pairwise correlation coefficients among representative bacterial genera, with hierarchical clustering based on co-abundance patterns. Color intensity reflects Pearson correlation coefficients. * indicates $P < 0.05$, ** indicates $P < 0.01$, *** indicates $P < 0.0001$.

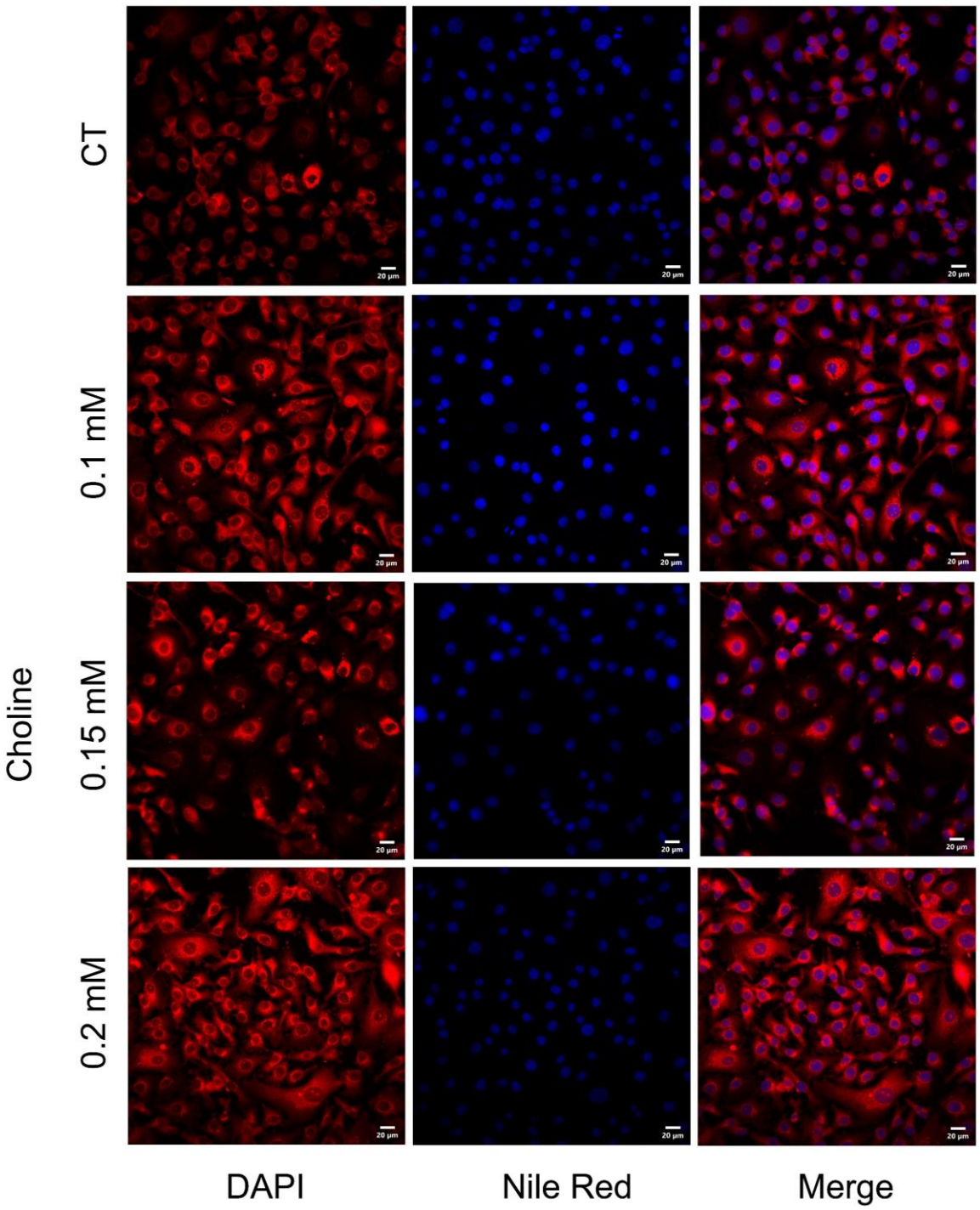

Figure S2. Effects of different concentrations of choline on the lipid accumulation in MAC-T cells, related to Figure 2.

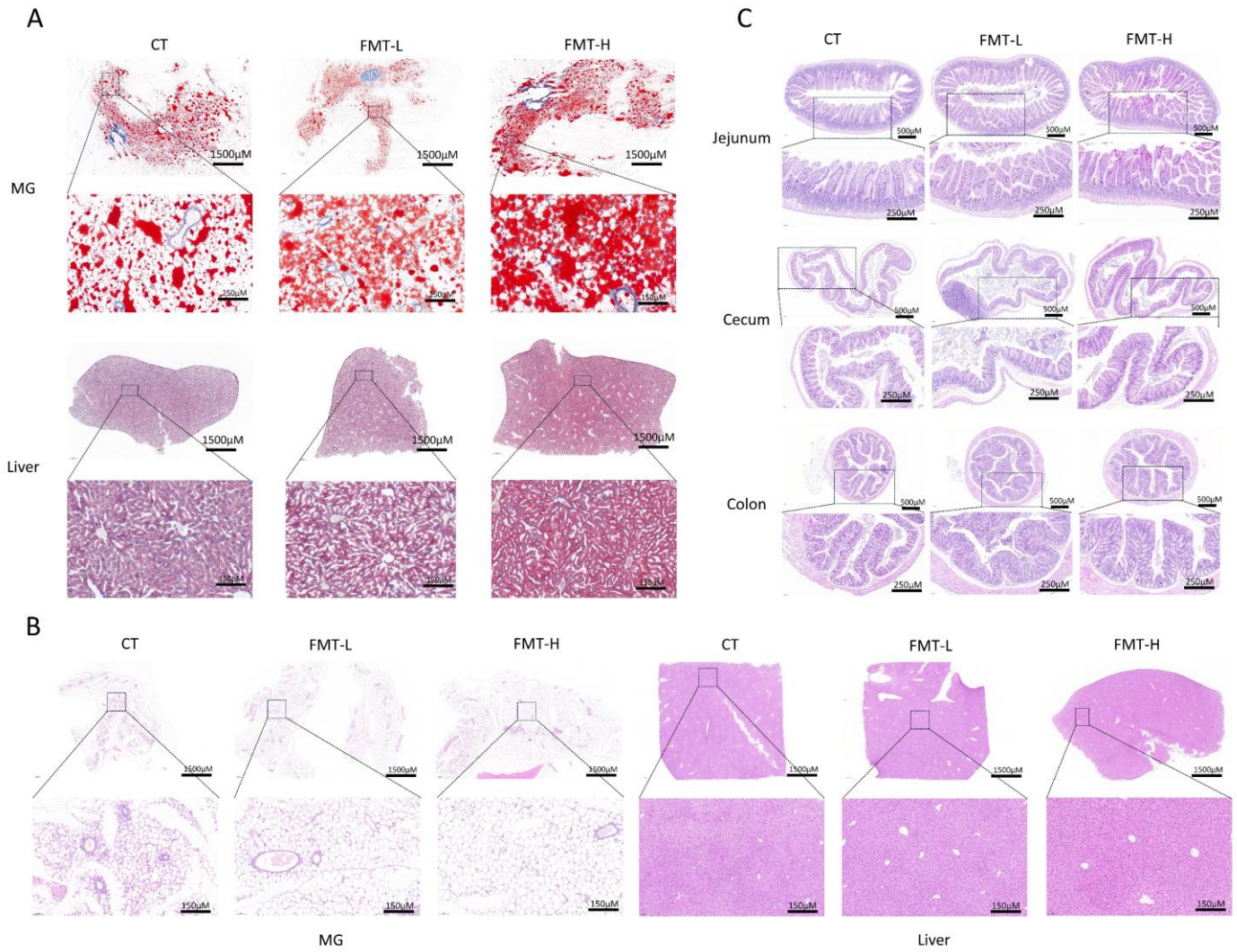

Figure S3 Tissue morphology in fecal microbiota transplantation-treated pregnant mice, related to Figure 3.

(A) Lipid accumulation in mammary gland (MG) and liver. Representative panoramic (top) and magnified (bottom) images of Oil Red O-stained MG sections demonstrate differential lipid deposition among control (CT), fecal microbiota transplantation from low milk fat yaks (FMT-L), and high milk fat yaks (FMT-H). Corresponding Oil Red O-stained liver sections are shown below. Scale bars: 1500 μm (panoramic), 250 μm (magnified). **(B)** Histological assessment of MG and liver tissues. Panoramic (top) and magnified (bottom) images of H&E-stained MG (left) and liver (right) sections reveal epithelial structure in MG and hepatic morphology across CT, FMT-L, and FMT-H groups. Scale bars: 1500 μm (panoramic), 250 μm (magnified). **(C)** Intestinal morphology. Representative H&E-stained sections of the jejunum, cecum, and colon from CT, FMT-L, and FMT-H groups. Both panoramic (top) and magnified (bottom) images are shown, highlighting mucosal integrity, villus structure, and crypt architecture in different intestinal regions. Scale bars: 500 μm (panoramic), 250 μm (magnified).

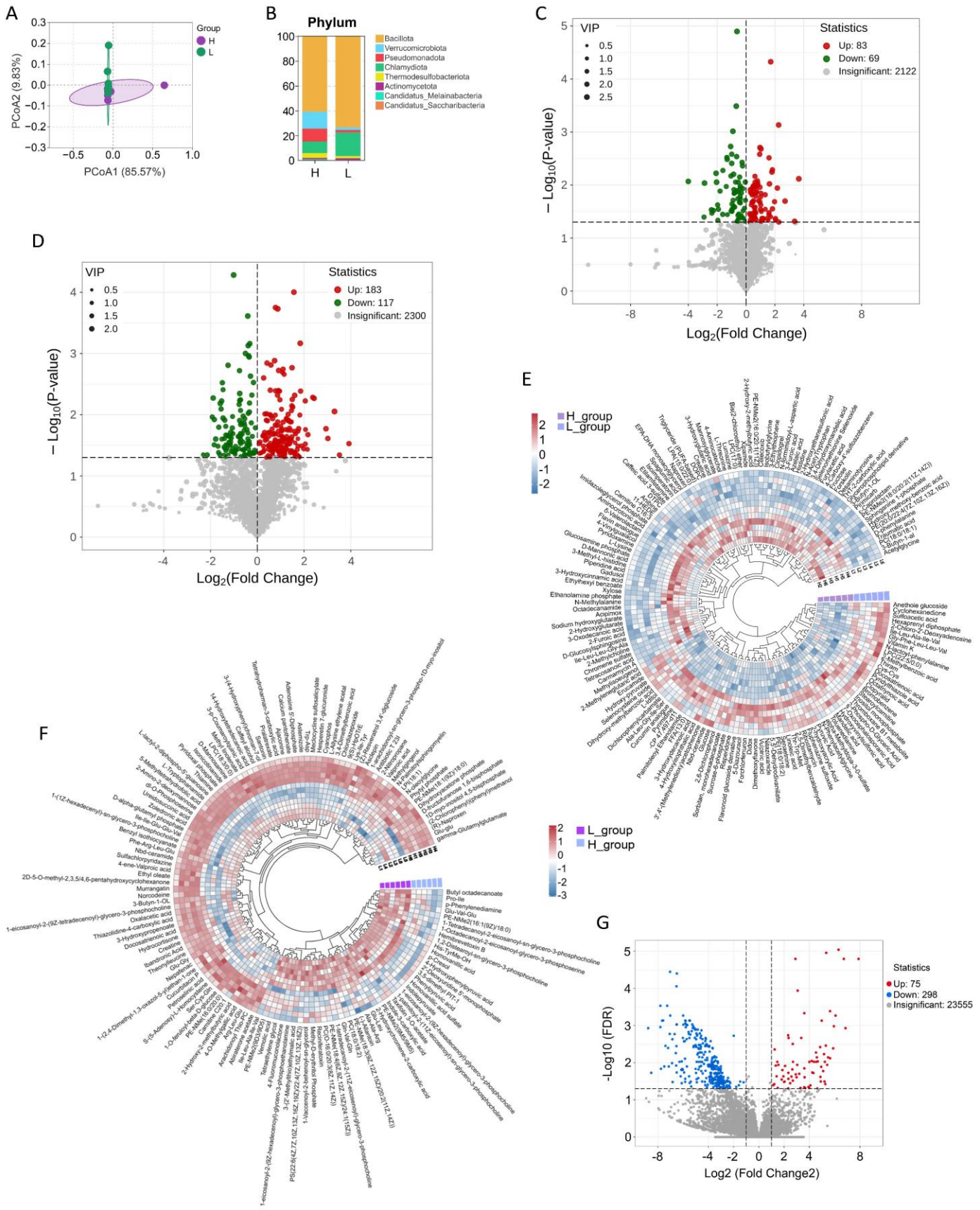

Figure S4. FMT reshapes gut microbiota and alters metabolic profiles in blood and mammary gland of pregnant Mice, related to Figure 4

(A) Principal coordinates analysis (PCoA) based on Bray-Curtis distances shows distinct clustering of gut microbiota between fecal microbiota transplantation (FMT)-treated pregnant mice receiving low milk fat percentage yaks (FMT-L) and high milk fat percentage yaks (FMT-H). **(B)** Relative abundance of bacterial phyla in fecal samples from FMT-H and FMT-L groups. **(C and D)** Volcano plots of differentially abundant metabolites of blood (C) and MG (D) between FMT-H and FMT-L groups.

Significantly upregulated (red) and downregulated (green) features were defined by VIP > 1 and $p < 0.05$; non-significant features are shown in gray. **(E and F)** Circular hierarchical clustering heatmaps of altered metabolites in blood (E) and MG (F) samples. Color scale indicates Z-score–normalized abundance across groups.

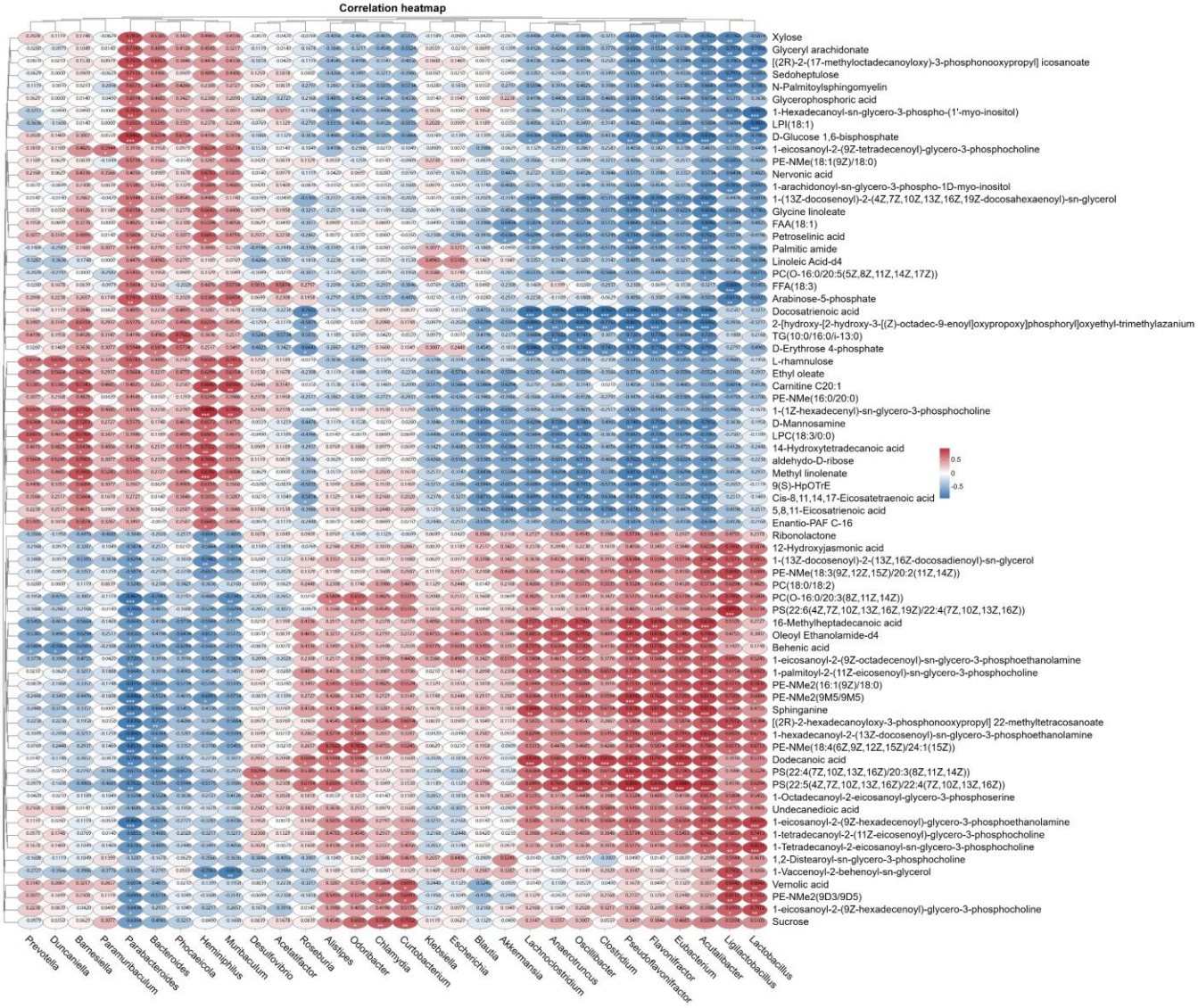

Figure S5. **Correlation between gut and blood metabolites, related to Figure 4.**

This heatmap illustrates the correlation between various metabolites in the gut and blood. The color scale represents correlation coefficients, with blue indicating negative correlations and red indicating positive correlations. The intensity of the color reflects the strength of the correlation. Each cell displays the correlation coefficient, with statistical significance denoted where applicable. Metabolites in the blood are listed on the y-axis, while gut microbiota-associated metabolites are shown on the x-axis. Statistical significance is indicated as follows: * $P < 0.05$, ** $P < 0.01$, *** $P < 0.001$.

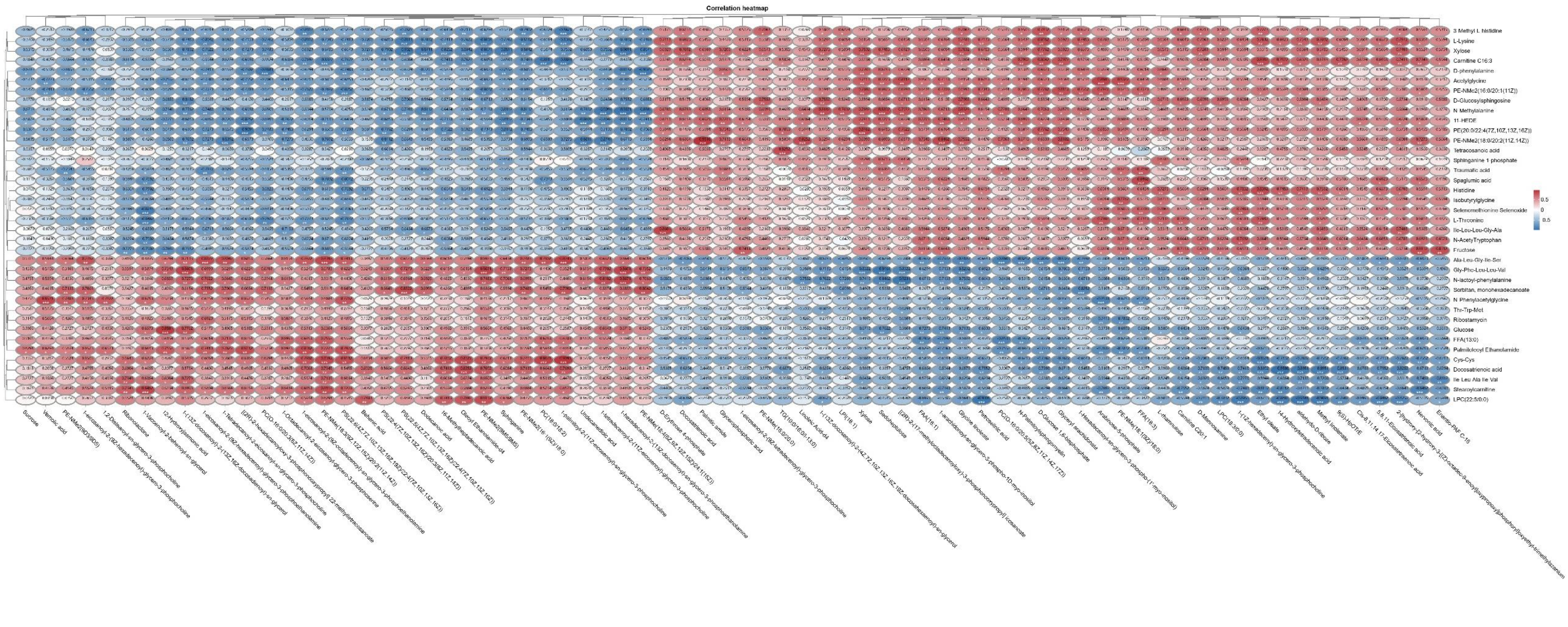
Correlation heatmap
3 Methyl L histidine
L-Lysine
Xylose
Carnitine C16:3
D-phenylalanine
Acetylglycine
PE-NMe2(16:0/20:1(11Z))
D-Glucosylsphingosine
N Methylalanine
11-HEDE
PE(20:0/22:4(7Z,10Z,13Z,16Z))
PE-NMe2(18:0/20:2(11Z,14Z))
Tetracosanoic acid
Sphinganine 1 phosphate
Traumatic acid
Spaglumic acid
Histidine
Isobutyrylglycine
Selenomethionine Selenoxide
L-Threonine
Ile-Leu-Leu-Gly-Ala
N-AcetylTryptophan
Fructose
Ala-Leu-Gly-Ile-Ser
Gly-Pro-Leu-Leu-Val
N-lactoyl-phenylalanine
Sorbitan, monohexadecanoate
N Phenylacetylglycine
Thr-Trp-Met
Ribostamycin
Glucose
FFA(13:0)
Palmitoleoyl Ethanolamide
Cys-Cys
Docosatrienoic acid
Ile Leu Ala Ile Val
Stearoylcarnitine
LPC(22:5/0:0)
0.5
0
0.5

Figure S6. Correlation between various metabolites in blood and the mammary gland.

This heatmap illustrates the correlation between various metabolites in the blood and mammary gland. The color scale represents correlation coefficients, with blue indicating negative correlations and red indicating positive correlations. The intensity of the color reflects the strength of the correlation. Each cell displays the correlation coefficient, with statistical significance denoted where applicable. Blood metabolites are listed on the x-axis, while mammary gland metabolites are shown on the y-axis. Statistical significance is indicated as follows: * $P < 0.05$, ** $P < 0.01$, *** $P < 0.001$.

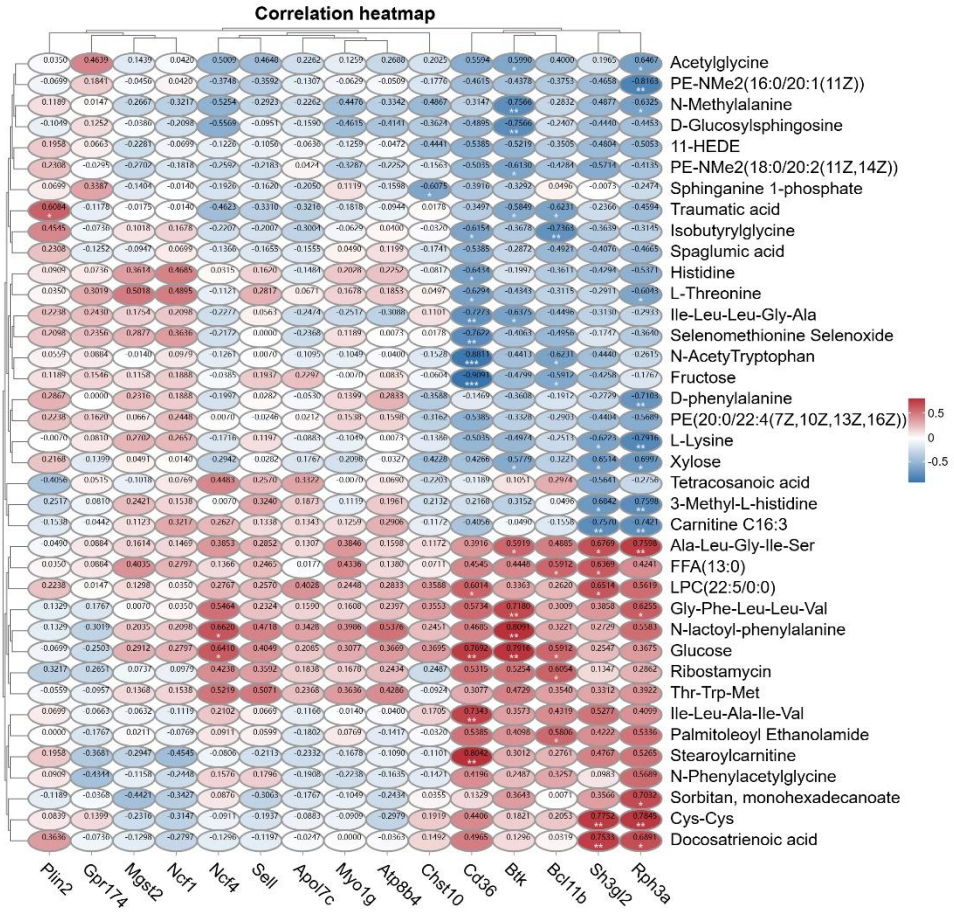

Figure S7. **Correlation between various metabolites and gene expression in the mammary gland.**

This heatmap illustrates the correlation between various metabolites and gene expression levels in the mammary gland. The color scale represents correlation coefficients, with blue indicating negative correlations and red indicating positive correlations. The intensity of the color reflects the strength of the correlation. Each cell displays the correlation coefficient, with statistical significance denoted where applicable. Metabolites are listed on the y-axis, while genes are shown on the x-axis. Statistical significance is indicated as follows: * $P < 0.05$, ** $P < 0.01$, *** $P < 0.001$.

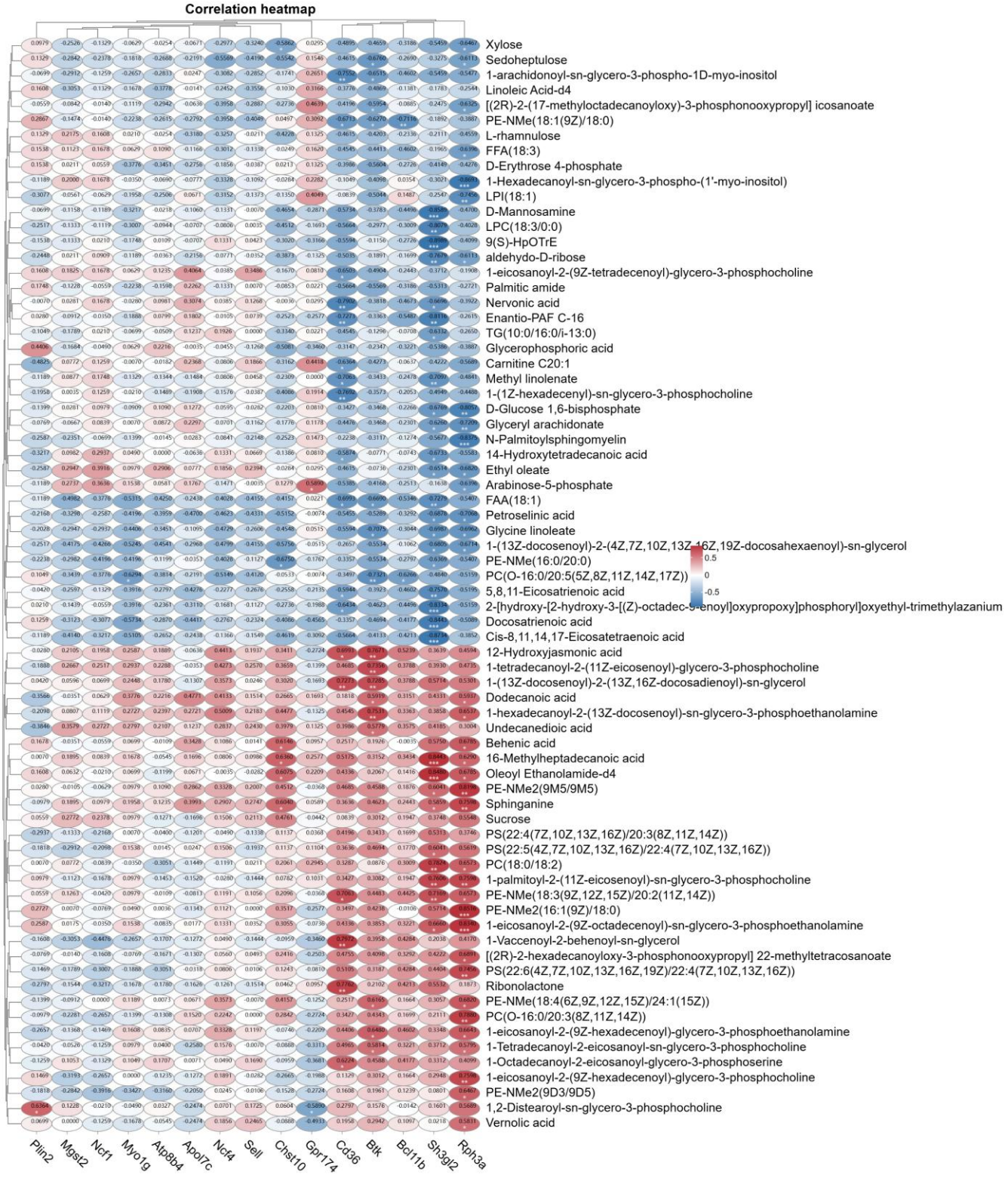

Figure S8. **Correlation between various blood metabolites and gene expression in the mammary gland.**

This heatmap illustrates the correlation between different blood metabolites and gene expression levels in the mammary gland. The color scale represents correlation coefficients, with blue indicating negative correlations and red indicating positive correlations. The intensity of the color corresponds to the strength of the correlation. Each cell contains the correlation coefficient value, and statistical significance is indicated where applicable. Metabolites are listed on the y-axis, while genes are represented on the x-axis. Statistical significance is indicated as follows: * $P < 0.05$, ** $P < 0.01$, *** $P < 0.001$.

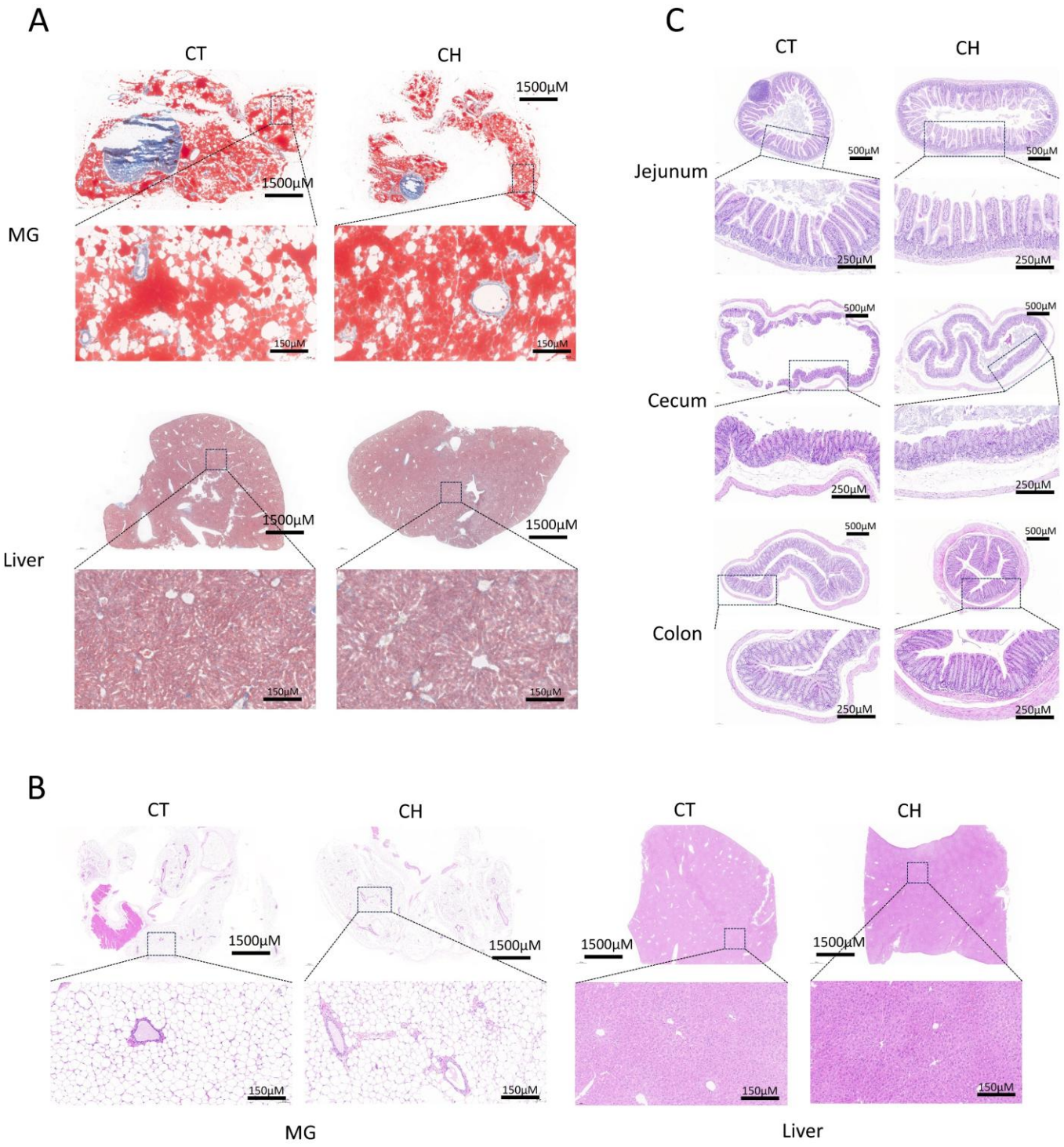

Figure S9. Tissue morphology in choline-treated pregnant mice, Related to Figure 6

(A) Lipid accumulation in mammary gland (MG) and liver. Representative panoramic (top) and magnified (bottom) images of Oil Red O-stained MG sections demonstrate differential lipid deposition among control (CT), choline-treated pregnant mice (CH). Corresponding Oil Red O-stained liver sections are shown below. Scale bars: 1500 μm (panoramic), 250 μm (magnified). **(B)** Histological assessment of MG and liver tissues. Panoramic (top) and magnified (bottom) images of H&E-stained MG (left) and liver (right) sections reveal epithelial structure in MG and hepatic morphology across CT and CH groups. Scale bars: 1500 μm (panoramic), 250 μm (magnified). **(C) Intestinal morphology.** Representative H&E-stained sections of the jejunum, cecum, and colon from CT and CH groups. Both panoramic (top) and magnified (bottom) images are shown, highlighting mucosal integrity, villus structure, and crypt architecture in different intestinal regions. Scale bars: 500 μm (panoramic), 250 μm (magnified).

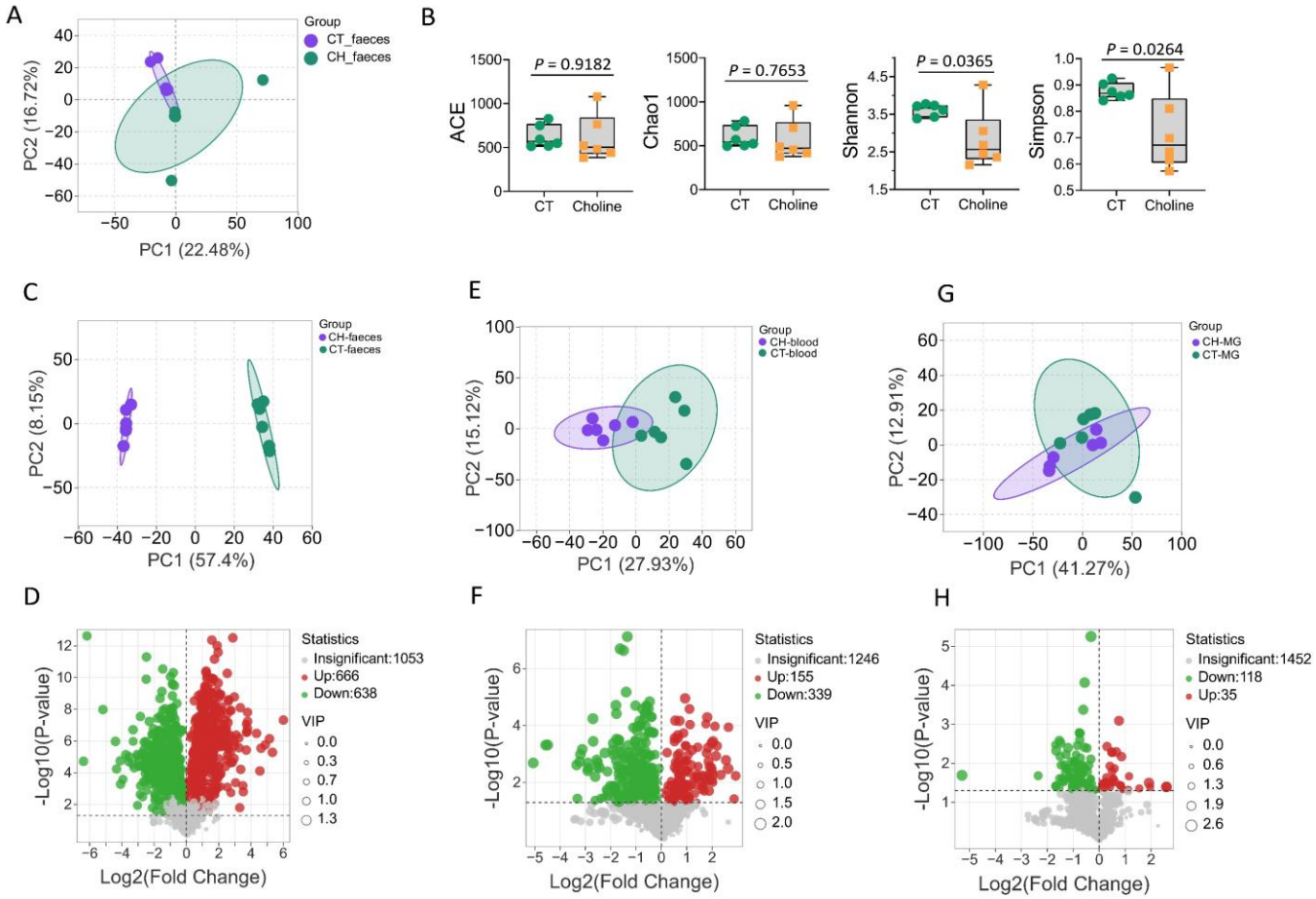

Figure S10. Choline supplementation alters gut microbiota composition and modulates metabolism of blood and mammary gland (MG) in pregnant mice, related to Figure 7.

(A) Principal Component Analysis (PCA) based on Bray-Curtis distance showing gut microbiota β-diversity differences between choline-treated (CH_faeces) and control (CT_faeces) mice. **(B)** Boxplots of α-diversity indices including ACE, Chao1, Shannon, and Simpson in fecal microbiota; Shannon and Simpson indices show significant differences between groups (P = 0.0365 and P = 0.0264, respectively; Wilcoxon test). **(C)** PCA of fecal metabolome profiles from choline-treated (CH_faeces) and control (CT_faeces) mice. **(D)** Volcano plot of fecal metabolites showing significantly upregulated (green) and downregulated (red) features in choline-treated mice. **(E)** PCA of serum metabolomic profiles showing separation between choline-treated (CH-blood) and control (CT-blood) mice. **(F)** Volcano plot displaying differentially abundant blood metabolites. **(G)** PCA of MG metabolomic profiles illustrating metabolic alterations induced by choline treatment. **(H)** Volcano plot showing differentially expressed metabolites in the mammary gland; red and green dots represent significantly decreased and increased metabolites, respectively.